Journal of Quantitative Spectroscopy & Radiative Transfer 293 (2022) 108390

Contents lists available at ScienceDirect

Journal of Quantitative Spectroscopy & Radiative Transfer

journal homepage: www.elsevier.com/locate/jqsrt

Absorption cross sections and local mode analysis for neopentane

Peter Bernath[a,b,*], Edwin L. Sibert III[c], Keith LaBelle[b], Jianbao Zhao[d], Brant Billinghurst[d]

[a] Department of Chemistry and Biochemistry, Old Dominion University, VA 23529, USA
[b] Department of Physics, Old Dominion University, VA 23529, USA
[c] Department of Chemistry and Theoretical Chemistry Institute, University of Wisconsin-Madison, Madison, WI 53706, USA
[d] Canadian Light Source Far-Infrared Beamline, 44 Innovation Blvd, Saskatoon, SK S7N 2V3, Canada

ARTICLE INFO

Article history:
Received 13 August 2022
Revised 13 September 2022
Accepted 2 October 2022
Available online 3 October 2022

Keywords:
Fourier transform infrared spectroscopy
Local mode analysis
Absorption cross sections
Neopentane

ABSTRACT

Spectra of neopentane, 2,2-dimethylpropane, $C(CH_3)_4$, were recorded in the 1200–1650 cm^{-1} region by high resolution Fourier transform spectroscopy at the Canadian Light Source (CLS) and converted to absorption cross sections. Samples were at 203, 233, 266 and 294 K with 0, 10, 30 and 100 Torr of nitrogen broadening gas. The previously published cross sections in the CH stretching region (2550–3350 cm^{-1}) [JQSRT 251, 107034 (2020)] were recalibrated and checked with two additional spectra recorded at Old Dominion University in the 1000–5000 cm^{-1} region. Local mode calculations for the CH stretching modes were carried out, and interactions with the overtones of the CH_2 scissor vibrations were included to obtain agreement with experiment.

1. Introduction

Neopentane (2,2-dimethylpropane, C_5H_{12}) belongs to a class of small hydrocarbons that includes methane, tetrahedrane [1] and adamantane [2] with tetrahedral symmetry. Although these molecules have no dipole moment, they have characteristic sharp Q-branches in their infrared vibrational spectra which aid in their detection. Small hydrocarbons such as methane and ethane are present in many planetary atmospheres including Earth [3], the giant planets [4] and particularly Titan [5], a moon of Saturn. Larger hydrocarbons such as benzene are formed by photochemistry and ion molecule chemistry in the upper atmosphere of Titan [6]. Neopentane is potentially present on Titan but infrared absorption cross sections are required for detection.

There has already been considerable work on the infrared and Raman spectra of neopentane [7–11] as well as calculations of vibrational structure [12,13]. Recently we recorded high resolution spectra in the 800–1600 cm^{-1} region and carried out local mode calculations to interpret the observations [14]. In a second paper, infrared absorption cross sections in the 2550–3350 cm^{-1} region were reported with nitrogen as a broadening gas [15], but the local mode analysis for the CH stretching modes was not published at that time. In this third paper, we now present high resolution absorption cross sections for the 1200–1650 cm^{-1} region with nitrogen as the broadening gas. The absorption cross sections reported in paper two were recalibrated and two additional spectra were recorded covering the 1000–5000 cm^{-1} region to check this recalibration. In addition, the local mode analysis was extended to cover the CH stretching region and used to interpret the spectra.

Neopentane has 45 normal modes and 19 fundamental frequencies of vibration, 3 of a_1 symmetry (ν_1-ν_3), 1 a_2 (ν_4), 4 e (ν_5-ν_8), 4 t_1 (ν_9-ν_{12}) and 7 t_2 (ν_{13}-ν_{19}), of which only the t_2 modes are infrared active [13,14]. In the 1200–1650 cm^{-1} region there are just 3 infrared active fundamental modes: ν_{17} (t_2) 1256.7 cm^{-1}, ν_{16} (t_2) 1369.4 cm^{-1} and ν_{15} (t_2) 1472.471 cm^{-1} [14]. There are 5 fundamental vibrational frequencies in the 2800–3000 cm^{-1} region: $\nu_1(a_1)$, 2909 cm^{-1}; $\nu_4(e)$, 2955 cm^{-1}; $\nu_9(t_1)$, (2942) cm^{-1}; $\nu_{13}(t_2)$, 2959.6 cm^{-1}; $\nu_{14}(t_2)$, 2876.2 cm^{-1}, but only 2 are infrared active [14].

1.1. Experimental method

High resolution infrared spectra of neopentane, pure and broadened by nitrogen, were recorded at the Canadian Light Source (CLS) Far Infrared Beamline with a Fourier transform spectrometer, similar to our previous work, e.g., [15,16]. Fig. 1 is an overview spectrum of neopentane at 203.5 K from 1240 to 1520 cm^{-1}. A 2 m base-path White-type cell with KBr windows was used with a nominal path length of 8 m at 4 temperatures and 3 N_2 broadening gas pressures (plus the pure sample): 203, 233, 266 and 294 K and 10, 30 and 100 Torr of broadening gas (total pressures). The samples were prepared by adding a small amount of neopentane to the cell, then adding the broadening gas and recording the total pressure. Pressures were measured with three recently calibrated

* Corresponding author at: Department of Chemistry and Biochemistry, Old Dominion University, VA 23529, USA.
E-mail address: pbernath@odu.edu (P. Bernath).

https://doi.org/10.1016/j.jqsrt.2022.108390
0022-4073/

Table 1
Experimental conditions for each spectrum.

Temp (K)	Neopentane (Torr)	Total (Torr)	Temp (K)	Neopentane (Torr)	Total (Torr)
203.55	0.0248	0.0248	266.25	0.0901	0.0901
203.55	0.0254	10.1	266.15	0.1056	10.2
203.55	0.0443	30.1	266.15	0.1647	30.0
203.55	0.0450	100.2	266.15	0.2705	100.7
Temp (K)	Neopentane (Torr)	Total (Torr)	Temp (K)	Neopentane (Torr)	Total (Torr)
232.95	0.0492	0.0492	293.65	0.1105	0.1105
232.95	0.0545	10.2	293.75	0.1666	10.2
232.85	0.0526	30	293.85	0.2161	30.0
232.95	0.0543	100.3	293.75	0.3012	101.5

Baratron pressure gauges (Model 127AA up to 1 Torr, Model 627B up to 10 Torr and Model 626B up to 1000 Torr). An SP Scientific model RC211 refrigerated re-circulating methanol bath cooled the cell. The cell temperature was monitored with 4 wire PT100 RTD (platinum resistance temperature detector) sensors with an estimated accuracy of ±2 K.

The CLS spectrometer was a Bruker IFS 125 HR Fourier transform instrument with a KBr beamsplitter, internal globar source, a 1200–1680 cm^{-1} band pass filter and a liquid N_2-cooled narrow band MCT (HgCdTe) detector. The spectral resolution varied depending on the total pressure: 0.0014 cm^{-1} (pure sample), 0.003 cm^{-1} (10 Torr), 0.01 cm^{-1} (30 Torr), and 0.04 cm^{-1} (100 Torr). The background spectra were recorded at 0.01536, 0.048, 0.048 and 0.048 cm^{-1} resolution, respectively, and Fourier interpolated to match the higher resolution spectra. The pressure and temperature parameters used for the samples are shown in Table 1. The cell was evacuated and refilled for each spectrum. For each spectrum, a minimum of 400 interferograms (200 forward and 200 backward) were co-added and boxcar apodization (i.e., no apodization) was used with a zero-filling factor of at least 8.

The CLS transmission spectra are converted to cross sections using [17]:

$$\sigma(\nu, T) = -\frac{10^4 k_B T}{Pl} \ln \tau(\nu, T)$$

in which $\tau(\nu, T)$ is the transmittance at wavenumber ν (cm^{-1}) and temperature T (K), P is the pressure of the absorbing gas in pascals (Pa), l is the optical path length (m), and k_B is the Boltzmann constant (1.380649 × 10^{-23} J/K). The path length used to calculate the cross sections was 8.63 m (including the total distance of 63 cm from the cell windows to the White cell mirrors). Residual water absorption lines were removed by hand.

The wavenumber calibration was carried out with an N_2O sample using reference line positions from the HITRAN database [18]. The calibration factor of 1.000000352(14) was applied to all spectra, which amounts to a shift of about 0.00045 cm^{-1} near 1300 cm^{-1}. After calibration, the wavenumber scale is accurate to better than 0.0001 cm^{-1}.

Cross sections for the CH stretching region were reported previously [15]. Based on spectra recorded at ODU, the pressure-pathlength was erroneously divided by a factor of 3. This factor of 3 has been removed and the cross sections have been recalculated.

The 16 infrared absorption cross section files for neopentane are available for the 1200–1650 cm^{-1} region along with the 16 recalibrated files for the 2550–3350 cm^{-1} region from the MoLLIST (Molecular Line Lists, Intensities and SpecTra) [19] web site http://bernath.uwaterloo.ca/molecularlists.php. Each cross section value (in cm^2/molecule) needs to be multiplied by 10^{-18}.

2. Results, local mode analysis and discussion

For the 1200–1650 cm^{-1} region (Fig. 1), the 16 new CLS neopentane spectra improve on the resolution and reach a lower temperature than the two ODU (Old Dominion University) spectra of pure samples analyzed previously [14]. Figs. 2–4 are expanded sections of Fig. 1 and show improvements compared to the corresponding Figures in the previous work [14] because of higher spectral resolution and lower temperature. The effect of the nitrogen broadening on the spectral features is illustrated in Fig. 5. The P(26) line in Fig. 5 is made up of a number of features due to "cluster" splitting from the partial lifting of the K degeneracy as the molecule rotates [20]. These cluster splittings are much better resolved in the new spectra (Fig. 5), and we have started a rotational analysis [21].

In addition to the spectra recorded at the CLS, two additional spectra were recorded at ODU to check on the recalibration of the

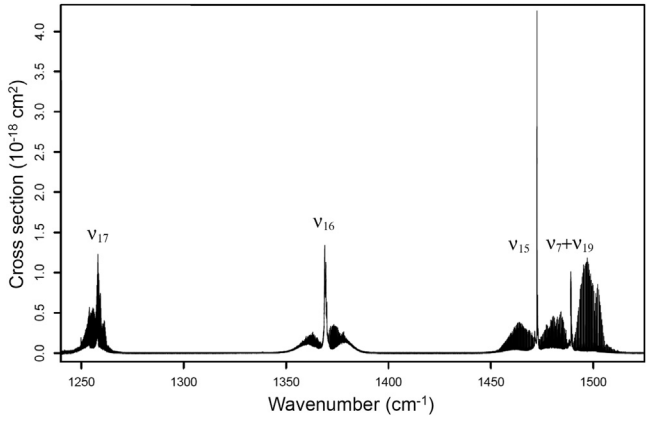

Fig. 1. Overview absorption cross sections of neopentane at 203.5 K with mode assignments [14].

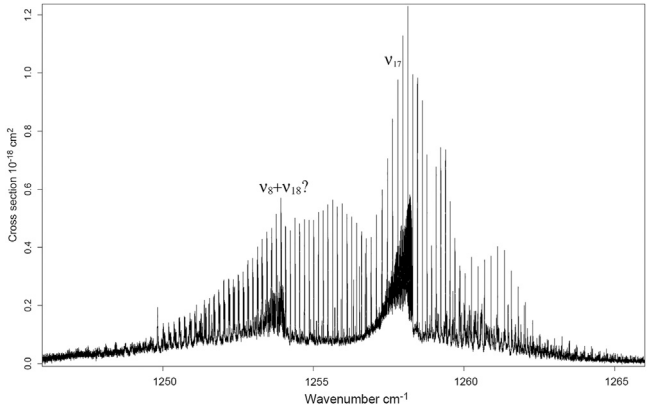

Fig. 2. Absorption cross sections of neopentane at 203.5 K for the ν_{17} fundamental and a weaker combination mode tentatively assigned as $\nu_8+\nu_{18}$ [14].

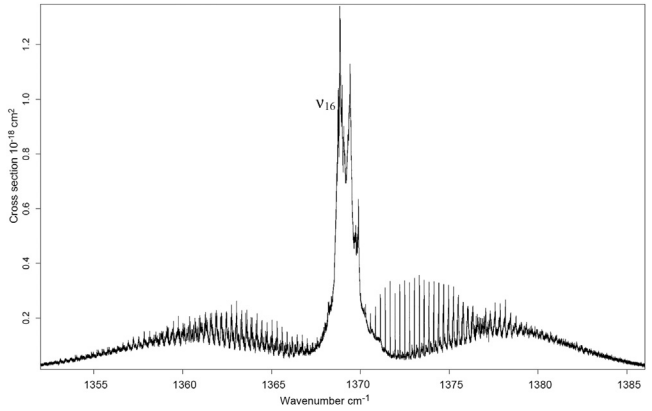

Fig. 3. Absorption cross sections of neopentane at 203.5 K for the ν_{16} fundamental [14].

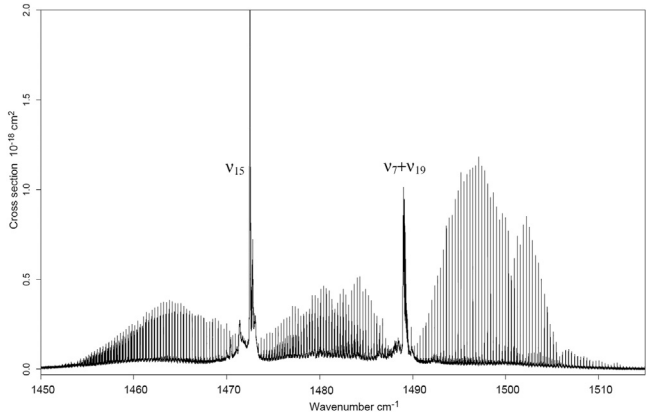

Fig. 4. Absorption cross sections of neopentane at 203.5 K for the ν_{15} fundamental and the $\nu_7+\nu_{19}$ combination mode [14]. The P branch of ν_{15} is from about 1455 to 1571 cm^{-1} to the left of the Q branch at 1472 cm^{-1} and the R branch of $\nu_7+\nu_{19}$ is from 1490 to 1512 cm^{-1} to the right of the Q branch at 1489 cm^{-1}, but the R branch of ν_{15} and the P branch of $\nu_7+\nu_{19}$ are mixed together from 1473 to 1488 cm^{-1}.

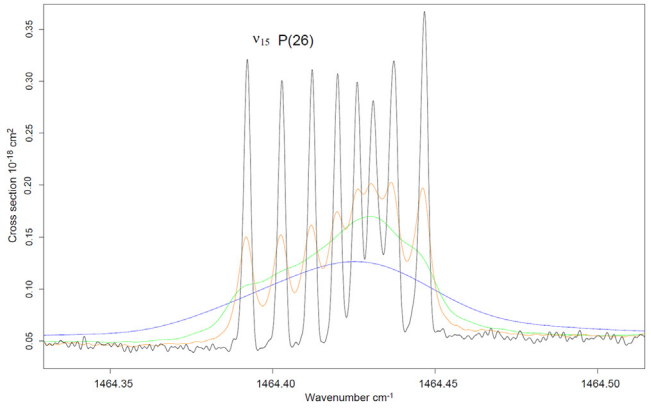

Fig. 5. The P(26) line of the ν_{15} (t_2) mode of neopenane at 203.5 K showing the cluster spittings and the effect of broadening by N_2 (black, pure neopentane; orange, 10.1 Torr; green, 30.1 Torr; and black, 100.2 Torr).

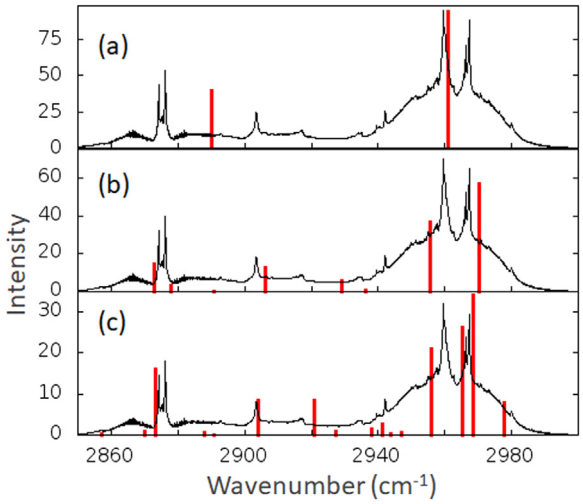

Fig. 6. Comparison of local mode stick spectra (red) to experimental (black) spectrum recorded at $T = 202$ K for three different levels of theory. (a) neglects Fermi coupling to CH_2 scissors, (b) neglects Fermi coupling of scissors to other low-frequency modes, and (c) full coupled. The units for the y-axes are km/mole; the calculated band strengths are for one of the 3 degenerate components of a t_2 mode. The experimental data have been scaled arbitrarity to fit in the panel.

cross sections in the CH region. The 1000–5000 cm^{-1} region was covered at a resolution 0.05 cm^{-1} with an MCT detector, a KBr beamsplitter, a Ge filter and a globar source. The 19.75 cm long cell with KBr windows was at 294 K and then cooled to 217 K for the second spectrum. The two ODU spectra were converted to cross sections and calibrated with the new room temperature cross sections recorded at the CLS. The 2660–3070 cm^{-1} region was then integrated and the areas were 60.1 cm/molecule (294 K) and 59.6 cm/molecule (217 K) cm/molecule compared to the average of 56.6 ± 0.6 cm/molecule for the recalibrated spectra. The difference of 5.7% is taken as an estimate of the error in the cross sections for the CH region.

The mean and standard deviation of the cross section area of an isolated band between 1335 cm^{-1} and 1400 cm^{-1} is 4.62 ± 0.08 cm/molecule. The estimate of the precision of the cross sections in the lower wavenumber region is therefore about 2%. However, there are no independent measurments for comparison so the overall accuracy is likely about 5–6%, similar to the higher wavenumber region.

The CH stretching region is more difficult to analyze than 1200–1650 cm^{-1} region: rotational analysis does not seem promising and even the vibrational structure is not clear. The scale for the y-axes of the figures in our second paper [15] need to be multiplied by a factor of 3. Only two strong allowed t_2 fundamental bands, $\nu_{13}(t_2)$, 2959.6 cm^{-1} and $\nu_{14}(t_2)$, 2876.2 cm^{-1}, are predicted in the C-H stretching region [14]. Additional bands appear because the overtone and combination bands of the scissors modes have Fermi resonance interactions with the C-H stretching modes [22,23]. As presented here, a local mode model that includes these interactions is in much better agreement with experimental observations.

The comparison of theory and experiment is shown in Fig. 6. The top panel shows the results of a CH stretch only calculation. With the local-mode model the transitions are predicted to occur at 2890.2 and 2961.1 cm^{-1} with intensities of 39.7 and 93.7 km/mol for each of the triplet components of the IR-active t_2 states. The local mode diagonal elements were scaled by 0.961. The corresponding B3LYP/6-311++(d,p) values from Gaussian [24] are 3009.0 and 3080.1 with intensities of 41.5 and 96.6 km/mol, respectively. The experimental conditions were reported previously [15]: the neopentane pressure was 30 mTorr at 202.15 K.

The results of Fig. 6(b) are the standard local-mode model results with Fermi couplings to the CH_2 scissors. The results are in qualitative agreement. In order to understand these results we note that there are 78 combination bands and overtones of scissor states with two quanta of excitation. While the local-mode Hamiltonian matrix is easy to construct and sparse, since the only anhar-

Table 2
Scissor combination states and their coupling matrix elements with the t_{2z} CH stretch states.

Symmetry	Basis state	Energy	V_1	V_2
$16(t_2)16(t_2)$		2721.5	-29.6	0.1
$2(a)16(t_2)$		2758.1	24.7	0.7
$10(t_1)16(t_2)$		2806.0	1.0	-9.4
$6(e)16(t_2)$		2816.4	1.0	6.5
$15(t_2)16(t_2)$	$\|1_{15x}1_{16y}\rangle + \|1_{15y}1_{16x}\rangle$	2842.7	2.9	4.1
$2(a)15(t_2)$	$\|1_2 1_{15z}\rangle$	2878.2	1.9	-6.9
$10(t_1)10(t_1)$		2889.6	-12.3	-5.9
$6(e)10(t_1)$	$\|1_{6b}1_{10z}\rangle$	2896.2	-15.9	7.9
$10(t_1)15(t_2)$	$\|1_{10x}1_{15y}\rangle - \|1_{10y}1_{15x}\rangle$	2921.2	18.1	2.0
$6(e)15(t_2)$	$\|1_{6a}1_{15z}\rangle$	2932.7	-7.8	-6.3
$15(t_2)15(t_2)$	$\|1_{15x}1_{15y}\rangle$	2959.6	-5.7	-7.5

monicities considered are those between states of the individual methyl goups [23], the analysis is difficult with this many states. For this reason, for our analysis we consider symmetry using a two step approach.

Following our standard approach we write the local-mode Hamiltonian as

$$H = H_{str} + H_{sci} + V. \quad (1)$$

Here V includes the stretch-scissor Fermi coupling terms that couple the CH stretch states to the CH_2 scissor overtone and combination modes. H_{str} describes 12 quadratically coupled CH local modes all with the same frequency; H_{sci} describes 12 quadratically coupled CH_2 scissor vibrations. At the harmonic level these local vibrations all have the same frequency, but the corresponding overtones are detuned from the combination modes by including a diagonal anharmonicity. Finally the overtones corresponding to vibrations on the same CH_3 group are allowed to couple *via* a Darling-Dennison resonance term. The details of these couplings have been described previously by Tabor et al. [23].

Rather than find the eigenvalues of this Hamilonian in terms of the local mode basis, we transform to an intermediate representation in which the basis set is a direct product of the stretch/scissor eigenstates of H_{str} and H_{sci}, respectively. The eigenvalues of the stretch and scissor Hamiltonians are found by diagonalizing H_{str} and H_{sci}, respectively. The diagonalization procedure automatically creates symmetrized states. However, whenever there are degeneracies, one must be careful to construct the proper linear combination. Linear combinations of the triply degenerate t_2 CH stretch states are carried out so that these triplets of states correspond to the *x*, *y*, and *z* components. A similar process is carried out for the scissor overtones and combination states. The anharmonicities included in the local-mode model remove many of the degeneracies, that are expected based on a harmonic analysis, and this manifold of states breaks up into 8a, 8e, and 18t states. This result is based on examining the degeneracies in the eigenvalues of H_{sci}.

Focusing on those states that are coupled to the t_{2z} IR-active CH stretch states, we find 11 scissor overtone and combination states that are coupled *via* the term V in Eq. (1). As the anharmonic terms in H_{sci} are relatively small, we use the normal mode labels to identify the eigenstates of H_{sci}. The 12 scissor fundamentals are $\nu_2(a_1)$, $\nu_{10}(t_1)$, $\nu_6(e)$, $\nu_{16}(t_2)$, $\nu_{15}(t_2)$. The first entry in Table 2 corresponds to a state with t_{2z} symmetry which is well-described as a state with two quanta of excitation in mode 16, a normal mode that has t_2 symmetry. The second column provides select information about the specific form of how scissor states are constructed to yield the correct overall t_{2z} symmetry. As an example, the combination state $15(t_2)16(t_2)$ is 9-fold degenerate in the harmonic limit. The state with t_{2z} symmetry is best described as the specific linear combination $|1_{15x}1_{16y}\rangle + |1_{15y}1_{16x}\rangle$ where the notation for each of the two basis states has one quantum of excitation in the modes that are indicated as subscripts. Table 2 also includes the corresponding energies as well as the couplings to each of the *z*-components of the two IR-active CH stretch states. Both V_1 and V_2 matrix elements are found by reexpressing the local mode stretch-bend Fermi couplings as couplings between the eigenstates of H_{str} and H_{sci}.

Table 2 reports the Fermi couplings V_1 (with state at 2890.2 cm^{-1}) and V_2 (with state at 2961.1 cm^{-1}) between the scissor states and the t_{2z} stretch states. Diagonalizing the 13 × 13 stretch/scissor Hamiltonian, whose elements are given in Table 2 along with the values of diagonal elements given directly above, leads to the same spectral results as diagonalizing the 90*x*90 local-mode matrix Hamiltonian.

At this level of theory and based on the energies of the stretch and scissor states one expects, and indeed one finds that the theoretical high-energy doublet (2955.7/2970.4 cm^{-1}) is well described as a linear combination of the CH stretch state with zero-order energy 2961.1 cm^{-1} and the combination band $|1_{15x}1_{15y}\rangle$ whose zero-order energy is 2960.5 cm^{-1}. The coupling is more complex at lower energies, with several states taking part in the mixing.

Although the agreement between theory and experiment is fairly good, in general there appear to be too few transitions predicted by theory. As an example, in the higher energy region, theory predicts a doublet, whereas the experiment shows three intense peaks consisting of a single and doublet at energies 2959.6, 2966.3, and 2976.4 cm^{-1}, respectively. Apparently there are additional mixings at play beyond those considered in our local-mode model.

Our earlier analysis of the CH_2 scissor fundamentals [14] points to a possible shortcoming of the model. In that work we found that the $\nu_{15}(t_2)$ band is strongly mixed with a background state. The mixing leads to two equal intensity peaks at 1472.5 cm^{-1} and 1489.0 cm^{-1}, respectively. Our calculation revealed that the background state is the combination band of the $\nu_7(e)$ and $\nu_{19}(t_2)$. The observed fundamentals of these two bands are 1060.0 cm^{-1} and 418 cm^{-1}, respectively. The cubic-coupling between the CH_2 scissor and the combination band was calculated numerically at the B3LYP/6-311++(d,p) level to be -8.7 cm^{-1} a value consistent with the observed splitting of 16.5 cm^{-1}. Following the notation of Raynes [25], the relevant coupling term is

$$V_F = F\left[\left(S_{15z}S_{19z} - \frac{1}{2}S_{15x}S_{19x} - \frac{1}{2}S_{15y}S_{19y}\right)S_{7a} + \frac{\sqrt{3}}{2}\left(S_{15x}S_{19x} - S_{15y}S_{19y}\right)S_{7b}\right] \quad (2)$$

There is a typo in our equation with this term in our previous paper [14]. The e_a and e_b were switched and a $\sqrt{3}$ on the z-component was missed. The subsequent matrix that we wrote down is correct as are the results. One can use those matrix results to include this Fermi interaction for all the states in Table 2 with excitation in mode 15. One finds that the state $|1_{6a}1_{15z}\rangle$ is coupled to the $|1_{6a}1_{7a}1_{19z}\rangle$ with a coupling of $F/\sqrt{8} = -8.7$ cm^{-1}. The highest energy state is more complicated, since there are two total quanta in mode 15. Here one must consider coupling between the scissor combination band $|1_{15x}1_{15y}\rangle$ and 7 other states $|1_{15x}1_{7a}1_{19y}\rangle$, $|1_{15x}1_{7b}1_{19y}\rangle$, $|1_{15y}1_{7a}1_{19x}\rangle$, $|1_{15y}1_{7b}1_{19x}\rangle$, $|2_{7b}1_{19x}1_{19y}\rangle$, $|1_{7a}1_{7b}1_{19x}1_{19y}\rangle$, $|2_{7a}1_{19x}1_{19y}\rangle$. For the diagonal energies of the 7 latter states we use experimental fundamental excitation energies and assumed we could sum the energies for the combination bands

The modified model increases the Hamiltonian describing the CH stretch region from a 13 × 13 matrix to a 24 × 24 matrix. The extra states are the above 7 plus one additional for each of the four other combination bands with excitation in mode 15. The spectral results are given in Table 3 and shown in Fig. 6. One observes improved agreement throughout the CH stretch spectral region. Note that the comparison of experiment with theory is qualitative be-

Table 3
Eigenstates (cm^{-1}) and intensities (km/mol) for the modified local mode Hamiltonian.

Energy	Intensity	Energy	Intensity
2715.9	1.3	2903.9	9.5
2754.3	0.9	2921.6	9.0
2806.3	0.3	2928.6	0.6
2816.1	0.2	2937.8	1.9
2832.3	0.2	2941.1	2.8
2857.2	0.5	2950.4	0.1
2869.3	8.6	2956.0	25.5
2871.1	6.7	2966.7	24.1
2887.8	0.1	2968.4	32.2
2889.6	0.5	2977.9	8.0

cause it is difficult to match the calculated and experimental features with certainty.

3. Conclusion and future plans

High resolution absorption cross sections of neopentane have been obtained in the 1200–1650 cm^{-1} region and cross sections in the 2550–3350 cm^{-1} region have been recalculated. These cross sections are useful for the search of neopentane in the atmosphere of Titan, although lower temperatures (150–195 K) are desirable [5]. A local mode model for the CH stretching region has been presented and is in reasonable agreement with observations. As usual for hydrocarbons, the overtone and combination modes of the scissors vibrations are in Fermi resonance with the CH stretching modes. An unusual feature of neopentane is that a key scissor vibration is also in Fermi resonance with other lower frequency modes. A rotational analysis of the vibrational bands in the 1200–1650 cm^{-1} region is planned.

Supplementary materials

Because of their size, cross section data files are available from the MOLLIST website (http://bernath.uwaterloo.ca/molecularlists.php).

Declaration of Competing Interest

The authors declare that they have no known competing financial interests or personal relationships that could have appeared to influence the work reported in this paper.

CRediT authorship contribution statement

Peter Bernath: Writing – original draft, Supervision. **Edwin L. Sibert III:** Writing – original draft, Formal analysis, Visualization. **Keith LaBelle:** Formal analysis, Data curation, Visualization. **Jianbao Zhao:** Data curation. **Brant Billinghurst:** Data curation.

Data availability

Data are available on MoLLIST website.

Acknowledgments

The NASA Outer Planets Research and Planetary Data Archiving and Restoration Tools program (PDART) provided funding (80NSSC19K0417). Part of the research described in this paper was performed at the Canadian Light Source, a national research facility of the University of Saskatchewan, which is supported by the Canada Foundation for Innovation (CFI), the Natural Sciences and Engineering Research Council (NSERC), the National Research Council (NRC), the Canadian Institutes of Health Research (CIHR), the Government of Saskatchewan, and the University of Saskatchewan. PB acknowledges RB for productive discussion. ELS gratefully acknowledges support from NSF *via* Grant No. CHE-1900095.

References

[1] Westbrook BR, Beasley GM, Fortenberry RC. Polycyclic aliphatic hydrocarbons: is tetrahedrane present in UIR spectra? Phys Chem Chem Phys 2022;24:14348. doi:10.1039/d2cp01103d.
[2] Pirali O, Boudon V, Oomens J, Vervloet M. Rotationally resolved infrared spectroscopy of adamantane. J Chem Phys 2012;136:024310. doi:10.1063/1.3666853.
[3] Helmig D, Rossabi S, Hueber J, Tans P, Montzka SA, Masarie K, et al. Reversal of global atmospheric ethane and propane trends largely due to US oil and natural gas production. Nature Geosci 2016;9:490–5. doi:10.1038/ngeo2721.
[4] Guerlet S, Fouchet T, Bézard B, Simon-Miller AA, Flasar FM. Vertical and meridional distribution of ethane, acetylene and propane in Saturn's stratosphere from CIRS/Cassini limb observations. Icarus 2009;203:214–32. doi:10.1016/j.icarus.2009.04.002.
[5] Hörst SMJ. Titan's atmosphere and climate. Geophys Res Planets 2017;122:432–82.
[6] Loison JC, Dobrijevic M, Hickson KM. The photochemical production of aromatics in the atmosphere of Titan. Icarus 2019;329:55–71. doi:10.1016/j.icarus.2019.03.024.
[7] Rank DH, Saksena BD, Shull ER. Vibrational spectra of carbon and silicon tetramethyl and their monodeutero derivatives. Disc Faraday Soc 1950;9:187–96. doi:10.1039/DF9500900187.
[8] Shull ER, Oakwood TS, Rank DH. Infrared and Raman spectra of tetramethylmethane-d_{12}. J Chem Phys 1953;21:2024–9. doi:10.1063/1.1698736.
[9] Murata H, Shimizu K. Normal frequencies of tetramethylmethane. J Chem Phys 1957;27:599–600. doi:10.1063/1.1743788.
[10] Sportouch S, Lacoste C, Gaufrès R. Spectres Raman du néopentane et du tétraméthylsilane à l'état gazeux. J Mol Struct 1971;9:119–27. doi:10.1016/0022-2860(71)85012-3.
[11] Weiss S, Leroi GE. Infrared spectra and internal rotation in propane, isobutane and neopentane. Spectrochim Acta 1969;25A:1759–66. doi:10.1016/0584-8539(69)80204-7.
[12] Schachtscheider JH, Snyder RG. Vibrational analysis of the n-paraffins-II. Normal co-ordinate calculations. Spectrochim Acta 1963;19:117–68. doi:10.1016/0371-1951(63)80096-X.
[13] Mirkin N, Krimm S. *Ab initio* analysis of the vibrational spectra of conformers of some branched alkanes. J Mol Struct 2000;550–551:67–91. doi:10.1016/S0022-2860(00)00513-5.
[14] Bernath PF, Sibert III EL, Dulick M. Neopentane vibrations: high resolution spectra and anharmonic calculations. J Phys Chem A 2020. doi:10.1021/acs.jpca.0c01723.
[15] Bernath P, Dodangodage R, Dulick M, Zhao J, Billinghurst B. Absorption cross sections for neopentane broadened by nitrogen in the 3.3 micron region. J Quant Spectrosc Rad Transf 2020;251:107034. doi:10.1016/j.jqsrt.2020.107034.
[16] Hewett D, Bernath P, Zhao J, Billinghurst B. Near infrared absorption cross sections for ethane broadened by hydrogen and nitrogen. J Quant Spectrosc Rad Transf 2020;242:106780. doi:10.1016/j.jqsrt.2019.106780.
[17] Harrison JJ, Allen NDC, Bernath PF. Infrared absorption cross sections for ethane (C_2H_6) in the 3 μm region. J Quant Spectrosc Radiat Transf 2010;111:357–63. doi:10.1016/j.jqsrt.2009.09.010.
[18] Gordon IE, Rothman LS, Hargreaves RJ, Hashemi R, Karlovets EV, Skinner FM, et al. The HITRAN2020 molecular spectroscopic database. J Quant Spectrosc Radiat Transf 2022;277:107949. doi:10.1016/j.jqsrt.2021.107949.
[19] Bernath PF. MoLLIST: molecular line lists, intensities and spectra. J Quant Spectrosc Rad Transf 2020;240:106687. doi:10.1016/j.jqsrt.2019.106687.
[20] Bernath PF. Spectra of atoms and molecules. 4th edition. New York, NY: Oxford University Press; 2020.
[21] Wenger C, Boudon V, Rotger M, Sanzharov M, Champion JP. XTDS and SPVIEW: graphical tools for the analysis and simulation of high-resolution molecular spectra. J Mol Spectrosc 2008;251:102–13. doi:10.1016/j.jms.2008.01.011.
[22] Bernath PF, Bittner D, Sibert III EL. Isobutane infrared bands: partial rotational assignments, *ab initio* calculations and local mode analysis. J Phys Chem A 2019;123:6185–93. doi:10.1021/acs.jpca.9b03321.
[23] Tabor DP, Hewett DM, Bocklitz S, Korn JA, Tomaine AJ, Ghosh AK, Zwier TS, Sibert III EL. Anharmonic modeling of the conformation-specific IR spectra of ethyl, *n*-propyl, and *n*-butylbenzene. J Chem Phys 2016;144:224310. doi:10.1063/1.4953181.
[24] Frisch MJ, Trucks GW, Schlegel HB, Scuseria GE, Robb MA, Cheeseman JR, et al. Gaussian 09. Wallingford CT: Gaussian, Inc; 2016.
[25] Raynes WT. Calculations of the force field of the methane molecule. Mol Phys 1987;60:509–25. doi:10.1080/00268978700100331.